Available online at www.sciencedirect.com
ScienceDirect
Journal of Power Sources 179 (2008) 723–733
JOURNAL OF POWER SOURCES
www.elsevier.com/locate/jpowsour

Experimental validation of a methanol crossover model in DMFC applications

Steffen Eccarius [a,*], Brenda Lee Garcia [b], Christopher Hebling [a], John W. Weidner [b]

[a] *Fraunhofer Institute for Solar Energy Systems ISE, Department of Energy Systems, Heidenhofstrasse 2, 79110 Freiburg, Germany*
[b] *Department of Chemical Engineering, University of South Carolina, Columbia, USA*

Received 24 September 2007; received in revised form 26 November 2007; accepted 29 November 2007
Available online 5 December 2007

Abstract

A design of experiments (DOEs) coupled with a mathematical model was used to quantify the factors affecting methanol crossover in a direct methanol fuel cell (DMFC). The design of experiments examined the effects of temperature, cathode stoichiometry, anode methanol flow rate, clamping force, anode catalyst loading, cathode catalyst loading (CCL), and membrane thickness as a function of current and it also considered the interaction between any two of these factors. The analysis showed that significant factors affecting methanol crossover were temperature, anode catalyst layer thickness, and methanol concentration. The analysis also showed how these variables influence the total methanol crossover in different ways due to the effects on diffusion of methanol through the membrane, electroosmotic drag, and reaction rate of methanol at the anode and cathode. For example, as expected analysis showed that diffusion was significantly affected by the anode and cathode interfacial concentration, by the thickness of the anode catalyst layer and membrane, and by the diffusion coefficient in the membrane. Less obvious was the decrease in methanol crossover at low cathode flow rates were due to the formation of a methanol film at the membrane/cathode catalyst layer interface. The relative proportions of diffusion and electroosmotic drag in the membrane changed significantly with the cell current of the cell.

Keywords: Direct methanol fuel cell; Modeling; Crossover; Characterization

1. Introduction

The portable electronic device market is placing increasing demands on battery technology to achieve higher energy and power densities. Portable fuel cells are one possible solution, allowing for longer runtimes and faster refueling [1]. As efficient storage of gases (e.g. hydrogen) is still a major obstacle in terms of weight, size, and safety, these portable fuel cells usually operate with liquid fuel. The liquid fuel is either reformed or directly converted into electrical energy. This paper will consider conversion of methanol to electric energy in a direct methanol fuel cells (DMFC).

In the power range up to several watts the fuel cell has to fulfill challenging requirements. For a DMFC system to be commercially viable, the energy density needs to be greater than $1000\,\mathrm{Wh\,l^{-1}}$ with a lifetime of at least 2000 h and operational costs below $5\,\$\,\mathrm{W^{-1}}$ [2].

In a DMFC, methanol is fed to the anode and air is fed to the cathode. Methanol is oxidized at the anode according to the following reaction

$$CH_3OH + H_2O \rightarrow CO_2 + 6H^+ + 6e^- \quad (1)$$

Oxygen from the air is reduced at the cathode via:

$$\tfrac{3}{2}O_2 + 6H^+ + 6e^- \rightarrow 3H_2O \quad (2)$$

In addition to being oxidized at the anode, some methanol also crosses the membrane where a portion of it is oxidized at the cathode according to Eq. (1) causing a mixed potential. Hence, the overall reaction that powers the DMFC system is:

$$CH_3OH + \tfrac{3}{2}O_2 \rightarrow CO_2 + 2H_2O \quad (3)$$

Fig. 1 shows a schematic of a direct methanol fuel cell that would be used for portable applications.

* Corresponding author. Tel.: +49 761 4588 5204; fax: +49 761 4588 9320.
E-mail address: steffen.eccarius@ise.fraunhofer.de (S. Eccarius).
URL: http://www.ise.fraunhofer.de (S. Eccarius).

0378-7753/$ – see front matter © 2007 Elsevier B.V. All rights reserved.
doi:10.1016/j.jpowsour.2007.11.102

Nomenclature

ACL	anode catalyst layer
AFC	anode flow channel
c	concentration (mol cm^{-3})
Ca	cathode
CBL	cathode backing layer
CCL	cathode catalyst layer
CCM	catalyst coated membrane
D	diffusion coefficient (cm^2 s^{-1})
DOE	design of experiments
GDL	gas diffusion layer
I	current density (A cm^{-2})
I_{cell}	cell current density (A cm^{-2})
I_{leak}	leakage current density (A cm^{-2})
k	mass transfer coefficient (cm s^{-1})
MEA	membrane electrode assembly
Mem	membrane
MeOH	methanol
MOR	methanol oxidation reaction
N	flux density (mol cm^{-2} s^{-1})
OCV	open circuit voltage
ORR	oxygen reduction reaction
Ox	oxygen
η	overpotential (V)
δ	thickness (cm)
ξ	electro-osmotic drag coefficient

One suggested method for simplifying the system and improving the energy density of DMFC system is to use a passive approach. In a passive approach, components like valves, pumps, heaters etc. are avoided to reduce losses of the system. As a consequence, passive DMFC systems are operated at or slightly above ambient conditions. A parasitic methanol oxidation at the cathode takes place because of a crossover of methanol from anode to cathode through the membrane. Methanol crossover decreases fuel efficiency and generates heat, which warms the fuel cell to temperatures slightly above room temperature. The extent of methanol crossover depends on design and operating conditions of the cell.

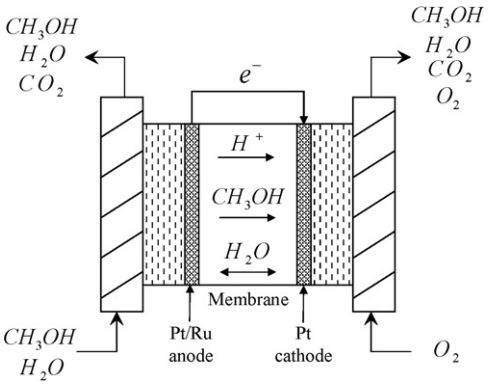

Fig. 1. Schematic of a single cell DMFC.

Several papers have been published that investigated the influence of a methanol crossover from anode to cathode in a solid polymer fuel cell. In a first approach Fuller et al. and Zawodzinski et al. studied the water uptake and transport through Nafion® 117 [3,4]. Later, methanol crossover and its influence on the cathode performance has been studied at elevated temperatures around 80 °C [5,6]. Heinzel et al. summarized the research on crossover in DMFCs in 1999 [7]. Lately some research has been done at near-ambient conditions [8,9].

In Meyers and Newman [10], a model for the methanol crossover was developed and the effect of methanol concentration was evaluated. Dohle et al. [11] and Garcia et al. [12] demonstrated 1-D isothermal models that predicted methanol crossover at different methanol concentrations. Jeng and Chen [13] developed a pseudo-2D model that predicts the total amount of methanol crossover in a DMFC for different methanol concentrations. Murgia et al. [14] used a 1-D model to predict the methanol crossover flux for different methanol concentrations and membrane thicknesses. Wang and Wang [15] used a CFD model to predict the individual contributions of diffusion and electroosmotic drag on methanol crossover for different currents.

In this paper, a design of experiments (DOEs) is coupled with 1-D model results to study the interaction of a significant number of design and operation parameters to understand their effect on methanol crossover. The design of experiments examined the effects of temperature, cathode stoichiometry, anode methanol flow rate, clamping force, anode catalyst loading, cathode catalyst loading (CCL), and membrane thickness as a function of current and it also considered the interaction between any two of these factors. As will be discussed below, the most significant factors affecting methanol crossover are temperature, anode catalyst layer (ACL) thickness, membrane thickness, and methanol concentration. Model analysis is used to understand how these factors influence the phenomena of electroosmotic drag and diffusion in the cell at different currents.

2. Experimental

2.1. MEA preparation

Nafion® was used as the ionomer for the MEAs. As the catalyst was put directly on the membrane the terminology of catalyst coated membrane (CCM) will be used in this paper. The catalyst layers of the CCM's were prepared in two steps [16]:

(1) Knife coating of the catalyst ink onto a decal foil.
(2) Transfer from the decal foil to either a Nafion®117 or Nafion® 1135 membrane by hot-pressing.

The anode catalyst consisted of 60 wt.% Pt/Ru and 40 wt.% carbon (Johnson Matthey 'HiSpec10000'). The Pt/Ru loading of the anodes was either 1.5 mg cm^{-2} or 2.5 mg cm^{-2} respectively. The cathode catalyst had a composition of 60 wt.% Pt and 40 wt.% carbon (Johnson Matthey 'HiSpec9000'), with a Pt loading of either 1.5 mg cm^{-2} or 2.5 mg cm^{-2}. All catalyst layers were prepared with a Nafion® content of 20 wt.%.

The hot-pressing temperature was 130 °C and the pressure 0.5 kN/cm^2.

2.2. Cell assembly

The test cell consisted of several parts, that could be modularly assembled. Anode and cathode plates were made out of a graphite compound BMA5 (SGL carbon) with the flowfield of the working electrode milled 0.8 mm deep into the graphite block. A thermo-couple was placed directly at the middle position of the working electrode on the backside of each graphite compound. The working electrode had an area of 10 cm^2 with 1 mm wide serpentine gas flow paths. By varying the thickness of the gaskets, different gas diffusion layers (GDLs) could be used. For this work SIGRAEC 31 BA GDLs (SGL carbon) were used for both, anode and cathode sides. The MEA was sandwiched between the GDLs and graphite blocks and the layers of this sandwich were aligned with four register pins. Two copper plates were used as current collectors on anode and cathode. The current collectors were pressed to the graphite block using two thick end plates made out of stainless steel. The temperature of the stainless steel plate was controlled by an external cryostat and distributed the temperature and pressure homogeneously over the whole assembly. Four springs were used in order to adjust the desired pressure on the MEA.

2.3. Measurement

The fuel cell was connected to a series of external devices. Methanol was supplied using a pulse free dosing pump, the gas flow for the cathode was adjusted by a mass flow controller. A reference cell was operated by two extra mass flow controllers with H_2 or air. The temperature on both endplates were controlled by a cryostat to guarantee isothermal conditions inside the cell. Current was drawn by an *Hcherl & Hackl Electronic Load ZS512*, which could be operated in constant current or constant voltage mode. Currents and voltages were recorded every 100 ms with the help of a data acquisition unit. The high frequency cell resistance was obtained using a *Agilent Milliohmmeter 4338B* which was recording the real part of the cell impedance at 1 kHz.

After a new fuel cell was assembled, it was conditioned by flooding the anode with distilled water over night. The electrodes were activated by supplying H_2 to the anode and humidified O_2 to the cathode while drawing a high current of up to 0.3 A cm^{-2} from the cell at 80 °C . Furthermore the fuel cell is preconditioned before each experiment: the cell potential was kept constant at 150 mV for approximately 10 min until it stabilized before switching back to the open circuit voltage (OCV). Polarization measurements were started at the OCV and the voltage was decreased in 25 mV-steps to short circuit with each step lasting 20 s. This measurement was repeated in order ensure no hysteresis effects were present. Polarization plots were extracted by averaging the sampled data of each operating point. Effects of the transient change between operating conditions were discarded by neglecting the initial 10 measurements. Standard deviation of the averaging procedure is displayed as error bars in each measurement.

Crossover measurements were performed by sampling the cathode exit gas each second using a mass spectrometer (MKS Mini-Lab). The pressurized air was analyzed in order to get the baseline for differential measurements. The CO_2-crossover from the anode to the cathode was determined in half cell operation of the DMFC. In the half-cell experiment, the cathode was potentiostated by flowing with hydrogen at a flowrate of 15 sccm. The absence of oxygen prevented methanol on the cathode side from being oxidized. For this case, all of the CO_2 measured in the cathode outlet stream must have crossed the membrane from the anode.

In addition to CO_2 crossing over from the anode, CO_2 is formed by the parasitic oxidation of methanol at the cathode (i.e. leakage current). The CO_2 and methanol were measured inside the cathode outlet stream during DMFC operation. All mass flows were converted to an equivalent current density using Faraday's law via reaction (1).

Table 1 depicts the eight independent variables used in the design of experiments with the two different values. A factorial design of the resolution V was applied, reducing the number of experiments from 2^8 to 64. In this design both the main effects and the two-factor interactions can be analyzed. Detailed reviews about the theory of a design of experiments can be found in Ref. [17]. Results of the DOE showed that a variation in the contact pressure by varying the clamping force had no influence for the given values and thus was neglected.

3. Model description

The methanol transport portion of the mathematical model developed by Garcia et al. [12,18] is extended to include oxygen diffusion through the cathode backing layer (CBL) and the assumption that all the MeOH that crosses to the cathode is completely oxidized at the cathode catalyst layer is relaxed such that some MeOH may pass through the cathode unoxidized. The CCL is modeled as an interface between the membrane and the CBL. Fig. 2 shows a schematic drawing of the different model domains.

The model includes a mass transfer resistance between the anode flow channel (AFC) and the anode backing layer (ABL) as described in Ref. [18]. It is an isothermal, steady-state model with variations only in one coordinate. CO_2 is assumed to be dissolved in solution. The anode kinetic expression is taken from

Table 1
Independent variables and their two values that are varied during the design of experiments

Independent variable	Value	Unit
MeOH concentration	0.5/1.5	M
Temperature	30/50	°C
Cathode stoichiometry	3/6	(min 40 sccm)
MeOH flowrate	1/3	ml min^{-1}
Clamping force	2/3.5	kN
Anode catalyst loading	1.5/2.5	mg cm^{-2}
Cathode catalyst loading	1.5/2.5	mg cm^{-2}
Membrane thickness	90/180	μm

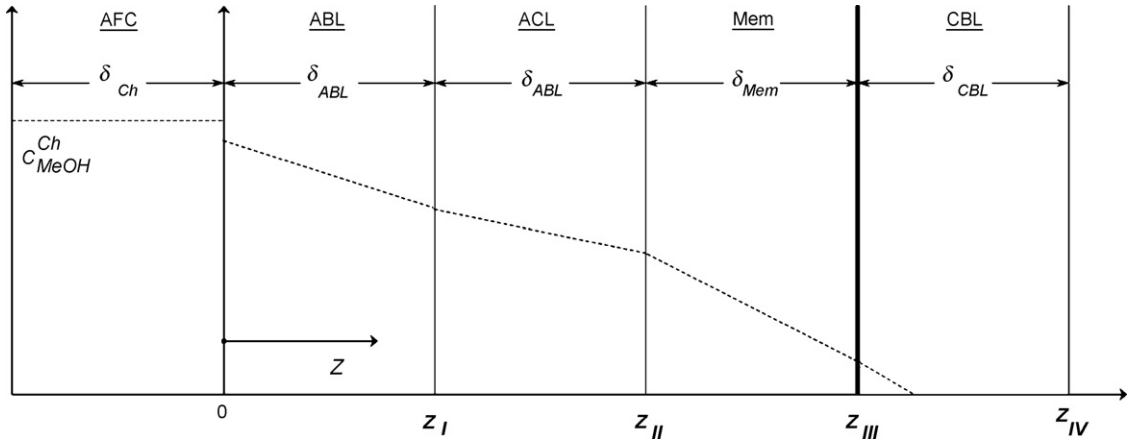

Fig. 2. Model domains that were used in the model. The CCL was modeled as an interface at z_{III}. An example for the relative MeOH concentration in the different model domains is shown.

[19] assuming a homogeneous reaction in the anode catalyst layer.

3.1. Methanol transport in the cathode

As will be shown later, a significant concentration of MeOH was measured in the cathode outlet stream during the experiments, even under open circuit conditions. This led to the conclusion that MeOH is not completely oxidized in the CCL but a small fraction leaves the CCL unreacted. In this work, it is therefore assumed that there can be transport of MeOH through the cathode, resulting in a MeOH concentration greater than zero within the CCL. This transport is described by a mass transfer coefficient in the CBL.

$$N_{\mathrm{MeOH,z_{IV}}} = k^{\mathrm{CBL}}_{\mathrm{MeOH}} \cdot c_{\mathrm{z_{III}}} \tag{4}$$

Consequently the flux of MeOH through the membrane in Ref. [12] is rewritten with the term $c_{z_{III}}$ for the MeOH concentration in the CCL.

$$N_{\mathrm{MeOH,z_{III}}} = \frac{(c_{\mathrm{z_{II}}} - c_{\mathrm{z_{III}}}) D^{\mathrm{Mem}}_{\mathrm{MeOH}}}{\delta_{\mathrm{Mem}}} + \xi \frac{c_{\mathrm{MeOH,z_{II}}}}{c_{\mathrm{H_2O,z_{II}}}} \cdot \frac{I_{\mathrm{cell}}}{F} \tag{5}$$

The flux of MeOH at position z_{III} is described by $N_{\mathrm{MeOH,z_{III}}}$. $D^{\mathrm{Mem}}_{\mathrm{MeOH}}$ denotes the MeOH diffusion coefficient in the membrane, δ_{Mem} the thickness of the membrane and I_{cell} the actual cell current, and ξ the electroosmotic drag coefficient. In addition to the diffusion term the electroosmotic drag with its coefficient ξ and the actual cell current I_{cell} is taken into account as well. The pressure on both sides of the fuel cell throughout experiments equaled atmospheric pressure. Thus this equation neglects the transport of MeOH across the membrane due to convection.

The leakage current density can be calculated according to Faraday's law via Eq. (5).

$$I_{\mathrm{leak}} = 6F(N_{\mathrm{MeOH,z_{III}}} - N_{\mathrm{MeOH,z_{IV}}}) \tag{6}$$

3.2. Oxygen transport in the cathode

Oxygenflux through the CBL to the CCL is modeled as a diffusion process through the CBL. The mass balance in the CBL is described as

$$\frac{\mathrm{d}N^{\mathrm{CBL}}_{\mathrm{O_2}}}{\mathrm{d}(z)} = 0 \tag{7}$$

The flux of oxygen through the membrane is assumed to be negligible. Oxygen is consumed inside the CCL according to the cell current density and the crossover current density.

$$N_{\mathrm{Ox,z_{III}}} = \frac{I_{\mathrm{cell}} + I_{\mathrm{leak}}}{4F} \tag{8}$$

Solving Eq. (7) for the CBL, one obtains

$$N_{\mathrm{Ox,z_{III}}} = \frac{(c_{\mathrm{Ox,z_{III}}} - c_{\mathrm{Ox,z_{IV}}}) D^{\mathrm{CBL}}_{\mathrm{O_2}}}{\delta_{\mathrm{CBL}}} \tag{9}$$

Here $c_{\mathrm{Ox,z_{IV}}}$ is the concentration of oxygen in the cathode flow channel. Using Eqs. (8) and (9) the concentration of oxygen inside the CCL can be determined. Knowing the oxygen concentration at the CCL a concentration term can be added to the Tafel equation for the oxygen reduction reaction (ORR).

$$I_{\mathrm{cell}} + I_{\mathrm{leak}} = I_{\mathrm{Ox},0} \cdot \frac{c_{\mathrm{Ox,z_{III}}}}{c_{\mathrm{Ox,z_{IV}}}} \exp\left(-\frac{\alpha_{\mathrm{Ca}} F \eta_{\mathrm{Ca}}}{RT}\right) \tag{10}$$

Losses occurring due to parasitic oxidation at the cathode are accounted for by I_{leak} from Eq. (6).

4. Results and discussion

4.1. Crossover experiments

Fig. 3 depicts one result of a cell operating at 30 °C and a 1.5 M solution of MeOH at a high air stoichiometry of 6. A total clamping force of 2850 N was applied, which creates a pressure of 285 kPa on the GDL. Nafion® 1135 was used with a catalyst loading of 2.5 mg cm^{-2} on both electrodes. $I_{\mathrm{CO_2,\ crossover}}$ stands for the equivalent current density of the CO_2 crossover from the anode to the cathode that was determined in half-cell experiments as described in the measurement section. In addition to CO_2, unreacted MeOH was found in the cathode outlet stream. The right axis refers to $I_{\mathrm{CO_2,\ crossover}}$ and $I_{\mathrm{MeOH,\ cathode\ exit}}$ while

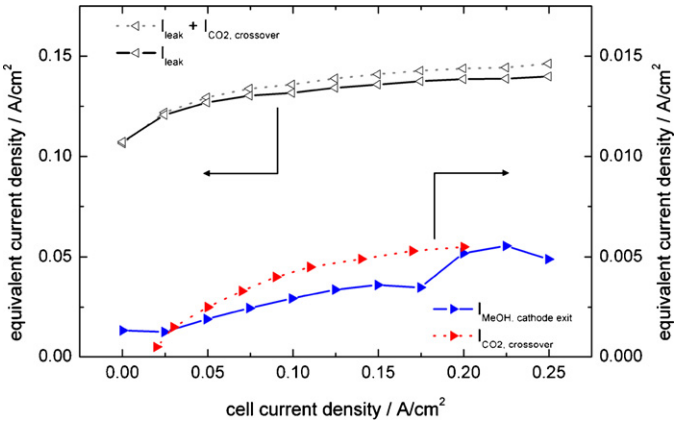

Fig. 3. Mass spectrometric measurements of the cathode outlet stream at a cell temperature of 30 °C, a 1.5 M MeOH solution, air stoichiometry 6, Nafion® 1135 and a catalyst loading of 2.5 mg cm^{-2} on both electrodes. The crossover of CO_2 from the anode to the cathode determined in half-cell experiments is labeled as $I_{CO_2,\,crossover}$, unreacted MeOH in full-cell operation as $I_{MeOH,\,cathode\,exit}$.

the total amount of CO_2 measured in the cathode outlet stream is plotted using the scale of the left axis. The leakage current can be calculated by subtracting $I_{CO_2,\,crossover}$ from the total CO_2 measurement at the cathode exit.

$$I_{leak} = I_{CO_2,\,cathode\,exit} - I_{CO_2,\,crossover} \quad (11)$$

It is shown in Fig. 3 that the MeOH on the cathode side is not completely oxidized, as MeOH is detected in small amounts in the mass spectrometer. The amount of MeOH exiting the cathode flux increases with increasing current. The CO_2 crossover measured during half-cell experiments and depicted as $I_{CO_2,\,crossover}$ stabilizes at a certain value and does not change significantly further on. It slightly changes the value of the leakage current density I_{leak} for a given cell current density. A relative error of 4% at a current density of 0.2 A cm^{-2}, caused by neglecting CO_2 crossover was calculated. In other experiments of the DOE, relative errors up to 20% were found.

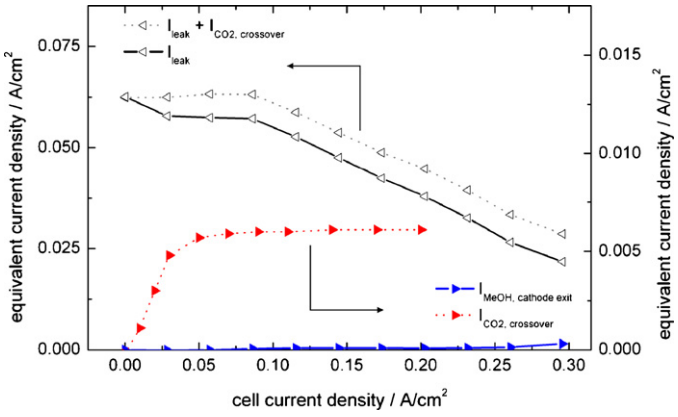

Fig. 4. Mass spectrometric measurements of the cathode outlet stream at a cell temperature of 50 °C, a 0.5 M MeOH solution, air stoichiometry 2, Nafion® 1135 and a catalyst loading of 2.5 mg cm^{-2} on both electrodes. The crossover of CO_2 from the anode to the cathode determined in half-cell experiments is labeled as $I_{CO_2,\,crossover}$, unreacted MeOH for full-cell operation as $I_{MeOH,\,cathode\,exit}$.

Fig. 4 illustrates another result with different operating conditions. The cell was operated at 50 °C with a 0.5 M solution of MeOH concentration and at a low air stoichiometry of 2. Again Nafion® 1135 was used with a catalyst loading of 2.5 mg cm^{-2} on both electrodes. No MeOH could be detected in the cathode outlet stream for this measurement. The CO_2 crossover stabilizes at about 0.006 A cm^{-2}. The relative error due to this can be calculated to be 18.5% at 0.2 A cm^{-2}. Thus, the impact of CO_2 crossover from the anode to the cathode should not be neglected in the evaluation of the measurement data [20,21].

A comparison between MeOH crossover in a full-cell experiment and a half-cell experiment is depicted in Fig. 5. The same operating conditions as in Fig. 3 were applied. For the half-cell experiment, all MeOH that was detected in the cathode outlet stream was converted into a current density. For the full-cell experiment the previously described method was used. The amount of MeOH in the cathode outlet stream was small and could be neglected.

It can be seen in Fig. 5 that the crossover current density of MeOH in the cathode outlet for the half cell experiment is one order of magnitude lower than for the CO_2 crossover current density in the full-cell experiment. Nevertheless, the slope of the two curves shows similar behavior. The crossover current density for the half-cell experiment starts close to zero and it can be concluded that the diffusive term of the crossover nearly vanishes. Therefore the gradient of the MeOH concentration between anode and cathode has to decrease. One phenomenon that could cause this is the formation of diluted MeOH, creating a liquid film on the pore walls of the CCL [22]. If a liquid film containing MeOH is formed on the cathode, the concentration gradient between ACL and CCL will decrease for all currents, thus reducing diffusion. The concentrations can equilibrate as the reductive hydrogen atmosphere at the cathode prevents MeOH from being oxidised and thus from being consumed. Evaporation of MeOH was low in the half-cell experiment because of a temperature of 30 °C and a low cathode flowrate of 15 sccm.

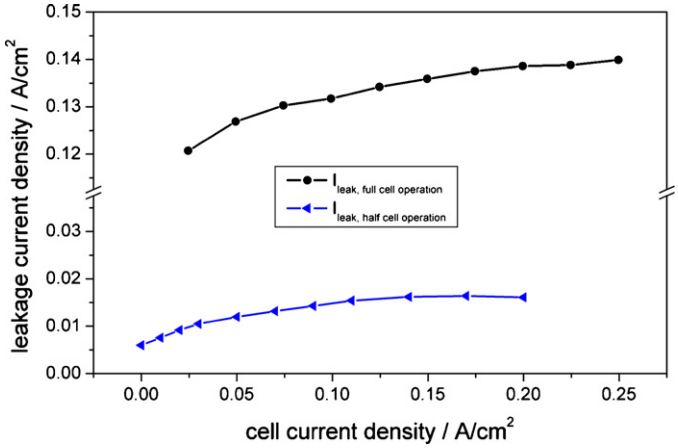

Fig. 5. Comparison of the equivalent MeOH crossover current density in half-cell and CO_2 crossover current density in full-cell experiments. The cell had a temperature of 30 °C, a 1.5 M MeOH solution, air stoichiometry of 6 for full-cell operation or a H_2 flow rate of 15 sccm for half-cell operation. Nafion® 1135 and a catalyst loading of 2.5 mg cm^{-2} on both electrodes was used.

4.2. Model validation

The assumption that all MeOH is oxidized at the Mem-CCL interface is often applied in DMFC modeling [5,13,23,15,11]. Even models that include a term for a MeOH transport concentration within the CCL in the cathode [24,25] assume the MeOH to be rapidly oxidized under given operating conditions and thus set the MeOH concentration at z_{III} to zero.

Experiments were performed to study whether the MeOH concentration at z_{III} was zero for all operating conditions. In these experiments, the fuel cell was operated at OCV while the MeOH concentration inside the AFC and the flow rate in the cathode flow channel were varied. These experiments were conducted using different concentrations between 0.2 M and 2 M in the anode. At OCV, the electroosmotic drag in Eq. (5) is zero. If the air or oxygen stream at the cathode inlet is high enough, then all the MeOH concentration at the CCL should go to zero as all of the liquid MeOH is either oxidized, evaporated or driven out by convection. Thus, at OCV and a high cathode flowrate, the crossover reaches a maximal flux and Eq. (5) can be reduced to

$$N_{\mathrm{MeOH},z_{III},\max} = \frac{(c_{z_{III}} - 0) D^{\mathrm{Mem}}_{\mathrm{MeOH}}}{\delta_{\mathrm{Mem}}} \tag{12}$$

The limiting parameters are the MeOH concentration at z_{II}, the diffusion coefficient within the membrane $D^{\mathrm{Mem}}_{\mathrm{MeOH}}$ and the thickness of the membrane δ_{Mem}.

Results from these experiments can be seen in Fig. 6. Nafion®117 was used at a cell temperature of 70 °C. Oxygen was supplied to the cathode at a back pressure of 2 bar. At lower cathode flow rates a strong increase of the leakage current density can be seen. At cathode flow rates above approximately 150 sccm, the MeOH flux from the anode to the cathode levels out at a certain value and depends only on the MeOH concentration within the AFC. This behavior at high flow rates is predicted by Eq. (12) assuming a well hydrated membrane with the same diffusion coefficient for all molarities. Thus, this method of MeOH crossover measurements at OCV with different MeOH concentrations can be used to determine the effective diffusion coefficient for MeOH crossing over from the ACL to the CCL in the Nafion® membrane. At cathode flow rates lower than 150 sccm, the crossover current density depends strongly on the flow rate of gas in the cathode. The formation of a liquid film on the cathode may explain the dependence of MeOH crossover on cathode flow rate at low current densities. A MeOH and water film on the cathode would reduce the concentration gradients of

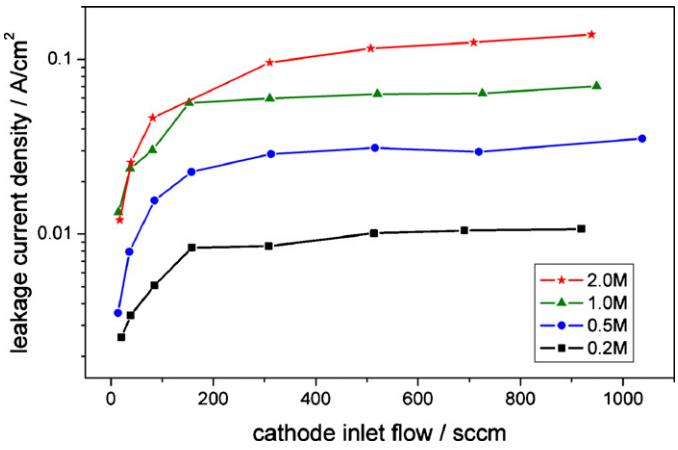

Fig. 6. Dependence of the flux of CO_2 in the cathode outlet stream on the cathode inlet flow for different MeOH solutions. No current was drawn from the fuel cell. The cell temperature was 70 °C, the back pressure was 2 bar and the anode flow rate 2 ml min^{-1}.

MeOH and water across the membrane, thus reducing crossover. In this case, this leads to the assumption that there is still a concentration $c_{z_{III}}$ of unreacted MeOH which forms a liquid film inside the CCL. The MeOH concentration $c_{z_{III}}$ varies depending on the mass transfer coefficient in the cathode.

The MeOH concentration at the Mem-CCL interface is not zero for all operating conditions. Model parameters for the diffusion coefficients can be found in Table 2. Values for the ACL and the membrane were taken from findings of Scott et al. [26], which agree reasonably well with calculated values from results shown in Fig. 6. The experimentally fitted value for the diffusion coefficient at the ABL was one order of magnitude higher than the values for pure diffusion in water. Thus it can be concluded that not only diffusional but also convectional forces were present inside the ABL throughout the experiments.

The dependence of the MeOH mass transfer coefficient in the cathode on the cell current density and the concentration of liquid MeOH inside the CCL has not been clarified yet. Furthermore, the flux of MeOH into the cathode outlet stream arbitrarily depended on structural parameters as well as operation conditions. The MeOH mass transfer coefficient in the cathode was also found to depend on MEA properties as well as operation conditions. In the model, the concentration of MeOH inside the CCL at $c_{z_{III}}$ and the MeOH mass transfer coefficient were assumed to be constant for all cell current densities. After allowing for this variation into the model, simulation results agreed

Table 2
Model parameters used for the simulation results, as e.g. depicted in Fig. 7

$D^{\mathrm{ABL}}_{\mathrm{MeOH}}$	Diffusion coefficient for MeOH in ABL (3.0×10^{-4} cm^2 s^{-1})	Fitted
$D^{\mathrm{ACL}}_{\mathrm{MeOH}}$	Diffusion coefficient for MeOH in ACL ($2.8 \times 10^{-5} \exp\left[2436\left(\frac{1}{353} - \frac{1}{T}\right)\right]$)	[26]
$D^{\mathrm{Mem}}_{\mathrm{MeOH}}$	Diffusion coefficient for MeOH in Mem ($4.9 \times 10^{-6} \exp\left[2436\left(\frac{1}{333} - \frac{1}{T}\right)\right]$)	[26]
$k^{\mathrm{CBL}}_{\mathrm{MeOH}}$	Mass transfer coefficient for MeOH in CBL (2×10^{-7} cm s^{-1})	Assumed
δ_{AFC}	Thickness of anode flow channel (0.1 cm)	Measured
δ_{ABL}	Thickness of anode backing layer (0.028 cm)	Measured
δ_{ACL}	Thickness of anode catalyst layer (0.002 cm)	Measured
δ_{Mem}	Thickness of membrane (0.018 cm)	Measured
δ_{CBL}	Thickness of cathode backing layer (0.03 cm)	Measured

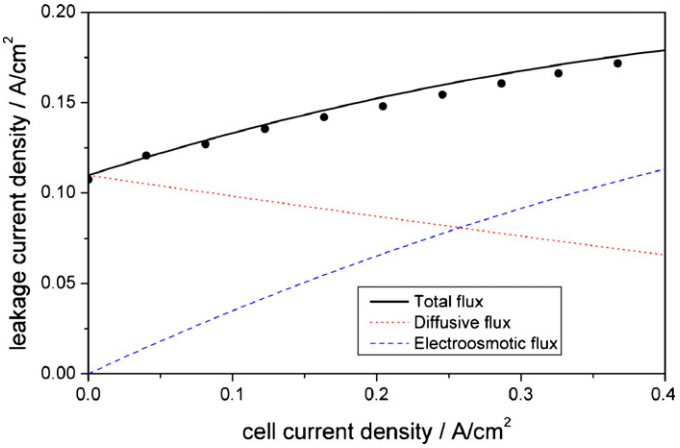

Fig. 7. Experimental and model results of the leakage current density and the contribution of diffusion and electroosmotic drag. Nafion® 117 with a catalyst loading of 2.5 mg cm^{-2} on both sides, 50 °C and a 1.5 M solution of MeOH was used. The anode flow rate was 3 ml min^{-1}, cathode stoichiometry was 6.

well with experiments as shown in Fig. 7. During operation of the fuel cell, electroosmotic drag causes crossover of MeOH as well. The cathode MeOH concentration at z_{III} and the electroosmotic drag coefficient were used as model parameters to fit measurement results to the model. The leakage current density at OCV where no electroosmotic drag occurred was used to fit $c_{z_{III}}$ to experimental values of the DOE. The electroosmotic drag coefficient was changed to fit the shape of the leakage current density as a function of different cell current densities data to experimental values.

One result of the fitting procedure can be seen in Fig. 7. The cell had a high catalyst loading of 2.5 mg cm^{-2} on both sides, Nafion®117, a temperature of 50 °C and a 1.5 M solution of MeOH was pumped at 3 ml min^{-1} to the anode. The cathode stoichiometry was 6. Experimental values of the leakage current density are displayed as dots. Fitting the proposed model to these data an electroosmotic drag coefficient of 2.2 was determined, which is in accordance with literature values [27]. The concentration of MeOH inside the CCL was found to be 0.56 M. Once these values had been determined, the different contributions of diffusion through the membrane, labeled as "diffusive flux", and the electroosmotic drag, labeled as "electroosmotic flux" of MeOH through the membrane, could be extracted from model results.

Table 3 documents mean values for experiments having the same operation conditions, specified in column two, and their standard deviation for the electroosmotic drag coefficient ξ and the concentration within the CCL $c_{z_{III}}$. The electrode catalyst loadings were equal for both sides, and the molarity and temperature were as specified in the operation condition column. The electroosmotic drag coefficient was found to be independent of all parameters except the temperature. The MeOH concentration inside the CCL depended on the molarity of the MeOH solution and the loading of the ACL.

A thicker ACL decreases the MeOH concentration at the interface z_{II} between the anode electrode and the membrane and hence reduces the MeOH concentration gradient between

Table 3
Values for the electroosmotic drag coefficient and the MeOH concentration inside the CCL with respect to feed concentration

Parameter	Operating conditions	Fitted simulation value	Standard deviation
ξ	30 °C	1.2	0.133
ξ	50 °C	2.3	0.197
$c_{z_{III}}$	1.5 mg cm^{-2}, 0.5 M	0.37 M (74%)	0.029 M
$c_{z_{III}}$	1.5 mg cm^{-2}, 1.5 M	1.20 M (80%)	0.188 M
$c_{z_{III}}$	2.5 mg cm^{-2}, 0.5 M	0.19 M (38%)	0.021 M
$c_{z_{III}}$	2.5 mg cm^{-2}, 1.5 M	0.56 M (37%)	0.050 M

Values were determined by fitting and averaging measurement results of the DOE to the proposed model and only changed with given operating conditions. Standard deviations from the averaging procedure are also presented.

z_{II} and z_{III}. Experimental results support this conclusion. At a high catalyst loading of 2.5 mg cm^{-2} (which equals a thickness of the ACL of 20 μm), the extracted values of $c_{z_{III}}$ were half of values calculated for a catalyst loading of 1.5 mg cm^{-2} (which equals a thickness of the ACL of 10 μm) for both the high and the low MeOH concentrations.

4.3. Influence of temperature

During the DOE, the leakage current density was measured at 30 °C and 50 °C. The results indicated that the electroosmotic drag was only a function of the temperature and no structural parameters, e.g. membrane thickness, showed an influence on the electroosmotic drag. The electroosmotic drag coefficient could be gained from model results as documented in Table 3. Extracted values are in good agreement with literature values [4,26,28]. The membrane model of Meyers et al. [19] predicts more open pores for liquid transport within the membrane at higher temperatures, which can be one cause for a higher drag coefficient at elevated temperatures. Ge et al. [29] has reviewed the literature from 4 different sources on the effect of temperature on the electroosmotic drag coefficient at different temperatures. He has shown that the electroosmotic drag coefficient increases linearly with temperature in a temperature range between 20 °C and 70 °C. He has also shown that the drag coefficient is independent of the cell current density.

Consequently, in this work the drag was assumed to increase linearly with temperature at the given temperature between 30 °C and 50 °C, the temperature range of the DOE. A linear extrapolation of the drag coefficient values at 30 °C and 50 °C was used in the model.

The predicted leakage current density at different temperatures can be seen in Fig. 8(a). The leakage current densities increase significantly with temperature, up to 0.1 A cm^{-2} were predicted with the maximum value at OCV and 70 °C. Black dots represent experimental values of the DOE. It can be noted that the increase of the leakage current density at small cell current densities is much higher compared to large cell current densities. Simulation results for the electroosmotic and diffusion parts of the leakage current density at OCV, 0.1 A cm^{-2}, 0.2 A cm^{-2}, 0.3 A cm^{-2} can be seen in Fig. 8(b) for a selection of temperatures.

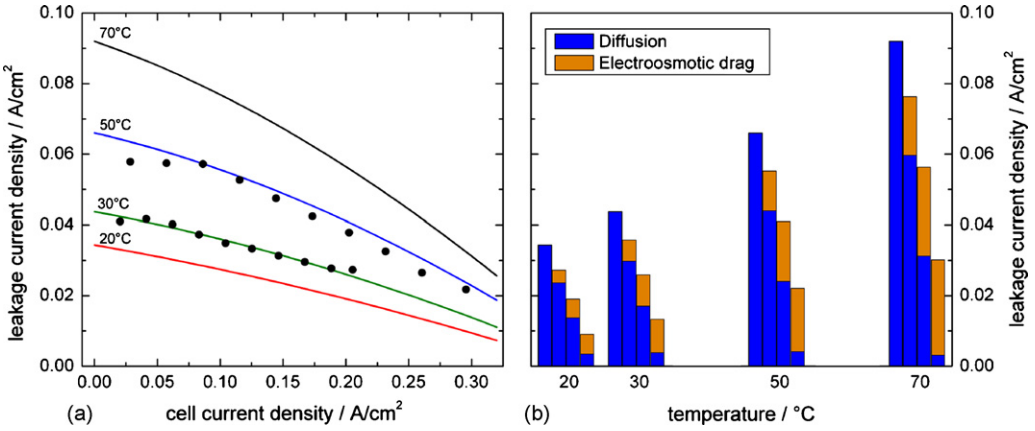

Fig. 8. (a) Simulation results for the leakage current density and experimental validation for Nafion®1135 with a catalyst loading of 2.5 mg cm^{-2} on both electrodes, a 0.5 M solution of MeOH flowing at 1 ml min^{-1} and an air stoichiometry of 2 at different temperatures. (b) Contributions of the electroosmotic drag and diffusion on the leakage current density. For each temperature, the values at OCV, 0.1 A cm^{-2}, 0.2 A cm^{-2}, 0.3 A cm^{-2} are displayed from left to right.

Obviously diffusion is the only driving force for the MeOH crossover at OCV. At 0.3 A cm^{-2}, the diffusion part of the leakage current density nearly vanishes and the leakage current density is dominated by the electroosmotic drag. At this current density, the MeOH concentration at z_{II} is nearly equal to the film concentration inside the CCL. The leakage current density at 0.3 A cm^{-2} is only one third of the leakage current density at OCV. Thus, Faradaic efficiency of the fuel cell operation at high cell current densities at near-ambient temperatures is favorable in terms of fuel economy.

4.4. Influence of membrane thickness

The thickness of the membrane influences crossover of MeOH to the cathode. The leakage current density for different membrane thicknesses can be seen in Fig. 9(a). Experimental values derived from the DOE for Nafion®117 (180 μm) and Nafion®1135 (90 μm) are depicted as dots and validate the model.

The different contributions of electroosmotic drag and diffusion are shown in Fig. 9(b). According to Eq. (5), the flux of MeOH at z_{III} at OCV is reciprocally inversely proportional to the membrane thickness δ_{Mem}. When a current is applied to the cell, the flux of MeOH to the cathode side increases due to electroosmotic drag and thus the MeOH concentration at z_{II} is lowered. In consequence, the concentration gradient of MeOH across the membrane between the ACL-Mem and CCL-Mem interfaces is lowered and the contribution of diffusion to the leakage current density decreases. It can be seen that for the given operating conditions, the diffusional part totally vanishes at cell current densities of 0.3 A cm^{-2}.

It can be concluded that fuel losses can be minimized by using thicker membranes. Especially at OCV or low current densities, the parasitic losses due to crossover of MeOH to the cathode can be minimized, optimizing the Faradaic efficiency.

4.5. Influence of molarity

While the electroosmotic drag coefficient changed the form of the function relating the leakage current density I_{leak} to the current density, the MeOH concentration inside the CCL $c_{z_{III}}$ determined the value of I_{leak} at OCV. The extracted model

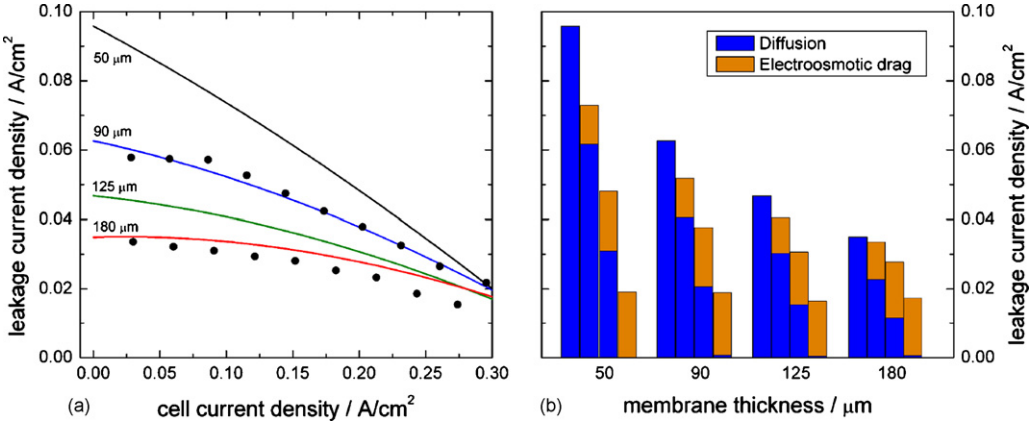

Fig. 9. (a) Simulation results for the leakage current density and experimental validation at a catalyst loading of 2.5 mg cm^{-2} on both electrodes, 50 °C, a MeOH concentration of 0.5 M at an anode flow rate of 1 ml min^{-1} and an air stoichiometry of 6 for different membrane thicknesses. (b) Contributions of the electroosmotic drag and diffusion on the leakage current density. For each membrane thickness the values at OCV, 0.1 A cm^{-2}, 0.2 A cm^{-2}, 0.3 A cm^{-2} are displayed from left to right.

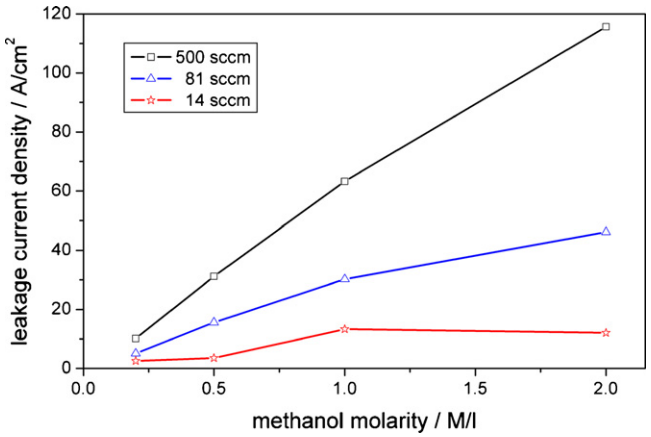

Fig. 10. Influence of the molarity on the leakage current density at different cathode flow rates. The operating conditions are as specified for Fig. 6.

parameters were compared for different changes of the MEA properties and changes of operating conditions in the DOE. As shown in Table 3, the MeOH concentration and the thickness of the ACL significantly influenced $c_{z_{III}}$ in the cathode. If no MeOH is consumed or evaporated inside the CCL and no current is drawn from the fuel cell, $c_{z_{III}}$ should equilibrate with the MeOH concentration of the AFC for the OCV. Thus for this limiting case, a strong dependence of the MeOH concentration of the AFC is expected. For the other limiting case, when all MeOH is consumed inside the CCL, only mass transfer resistances control the flux. Therefore a thicker ACL acts as a larger barrier for MeOH to cross to the CCL and decreases the flux of MeOH.

As the electroosmotic drag vanishes at OCV, MeOH permeates through the membrane only by diffusion. Fig. 10 shows the leakage current density for different molarities and cathode air flow rates. The leakage current density shows a linear behavior on the MeOH concentration in the feed and declines with the cathode flow rate. A linear dependence between MeOH concentration in the feed and MeOH concentration at z_{III} is assumed in the given range, an assumption that holds true if consumption of MeOH at z_{III} is constant for different molarities. Values extracted from experimental results at 0.5 M and 1.5 M are extrapolated and introduced into the model.

Simulation results for the leakage current density at various MeOH concentrations can be seen in Fig. 11(a). At 0.5 M and 1.5 M it was validated using experimental values of the DOE. Simulation results at a MeOH concentration of 4 M have to be regarded as a qualitative projection as the linear dependence was not verified for concentrations greater than 2 M. The molarity has a much higher impact on the leakage current density than the temperature (Fig. 8) or the membrane thickness (Fig. 9). It also changes the gradient from a decrease with cell current density at lower MeOH concentrations to rising values at higher concentrations. The cause can be seen in Fig. 11(b). Although the diffusion part of the leakage current density is decreasing with increasing cell current density at MeOH concentrations greater than 0.5 M, the superposition of diffusion and electroosmotic drag is increasing. The ratio of drag to diffusion rises with cell current densities. For MeOH concentrations greater than 0.5 M, it increases only slightly with MeOH concentration.

In conclusion, it is favorable to operate a LDMFC at lower MeOH concentrations, especially at the interface between ACL and membrane, to keep crossover small. For higher MeOH concentrations, the crossover even increases with cell current density. At 4 M and 0.3 A cm^{-2} the leakage current density exceeds the cell current density by a factor of almost two.

4.6. Influence of anode flow rate

During the DOE, experiments were performed at a flow rate of 1 ml min^{-1} and 3 ml min^{-1} to study the influence of anodic flow. Results indicated that the flow rate of MeOH at in the anode had an noticeable impact on the crossover. This was introduced as a dependence on flow rate for the mass transfer between the anode flow channel and the backing. The model was tested with parameters fixed to a 0.5 M solution of MeOH at 30 °C and a thickness of 90 μm. The flow rates was parameterized between 0.5 ml min^{-1} and 7 ml min^{-1}.

To verify the model predictions, additional experiments were performed at OCV and different anode flow rates. Fig. 12 shows

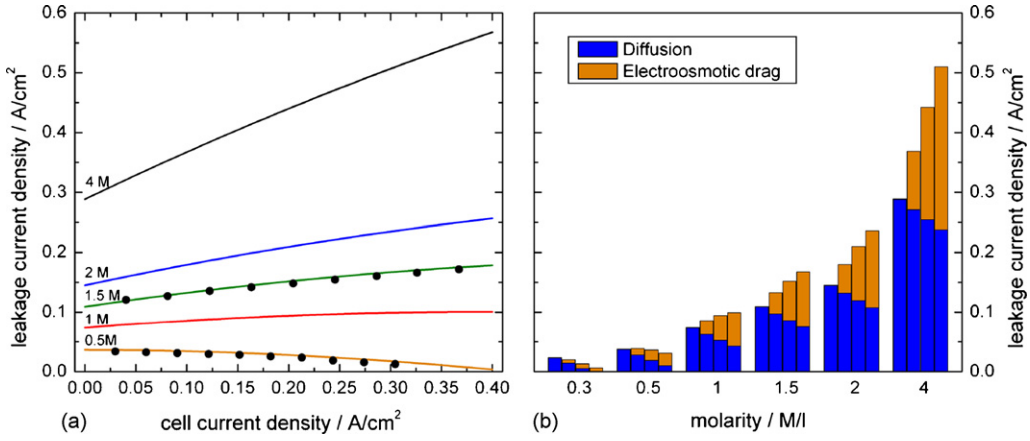

Fig. 11. (a) Simulation results for the leakage current density and experimental validation for Nafion® 117 with a catalyst loading of 2.5 mg cm^{-2} on both electrodes, 50 °C, an anode flow rate of 1 ml min^{-1} and an air stoichiometry of 6 at different molarities. (b) Contributions of the electroosmotic drag and diffusion on the leakage current density. For each molarity the values at OCV, 0.1 A cm^{-2}, 0.2 A cm^{-2}, 0.3 A cm^{-2} are displayed from left to right.

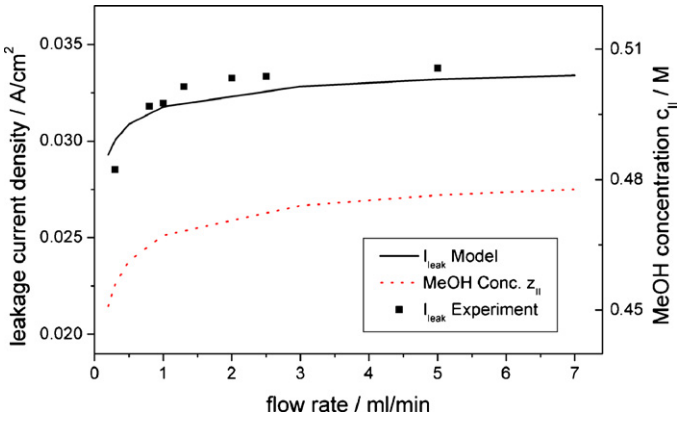

Fig. 12. Simulation results and experimental values for the total leakage current density and the MeOH concentration at z_{II} at OCV and varying flow rates. A 0.5 M solution of MeOH and Nafion® 1135 having a catalyst loading at each electrode of 2.5 mg cm^{-2} at 30 °C was used. Air was supplied to the cathode at a constant flow rate of 20 sccm.

experimental values for Nafion ® 1135 having a catalyst loading at each electrode of 2.5 mg cm^{-2}, the same operating conditions as for the simulation. Air was supplied to the cathode at a constant flow rate of 20 sccm. The model agreed well with the experimental values. As can be seen in the model predictions, the leakage current density at OCV increases sharply at first an then goes into saturation as the anode flow rate is increased. On examining the modeled MeOH concentrations at the ACL/membrane interface, it is obvious that a decreases at low flow rates in the MeOH concentration is the cause for the lower leakage current densities at low flow rates.

Changing the anode flow rates leads to a significant change in the shape of the total leakage current density on the cell current density as model predictions indicate in Fig. 13. Here the total crossover density and the contributions of electroosmotic drag and diffusion are plotted for a MeOH flow rate of 0.5 ml min^{-1}and 7 ml min^{-1}respectively. It is obvious that the superposition of drag and diffusion leads to different behavior on the leakage current density, depending on which process dominates. For a high anode flow rate, the crossover slowly decreases with increasing current density, whereas it strongly decreases for the lower flow rates. Therefore, one can conclude that for high power densities or high current densities, a low MeOH flow rate is preferable with respect to the MeOH crossover.

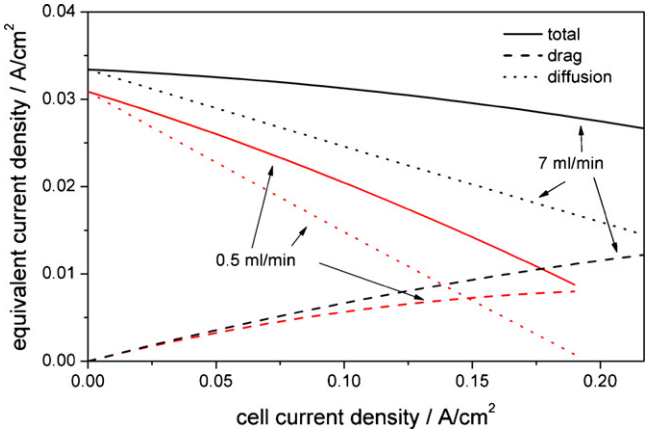

Fig. 13. Simulation results for the leakage current density at 30 °C and a membrane thickness of 90 μm. The shape of the total leakage current density changes significantly between 0.5 ml min^{-1} and 7 ml min^{-1} due to much lower MeOH concentrations at z_{II} for low flow rates.

In addition to the model results, it is possible that a pressure difference between the anode and cathode compartment, which was neglected in the model, is more pronounced at higher flow rates and consequently causes higher leakage current densities [30,31].

5. Conclusions

An analytical one dimensional model for a DMFC was enhanced to describe crossover of methanol from anode to cathode. It was shown experimentally that at OCV crossover increased with cathode flowrate, depending on molarity. Furthermore unreacted methanol was detected in the cathode outlet stream besides oxidised CO_2. Thus it was assumed in the model that at low cathode flow rates concentration inside the cathode catalyst layer was non-zero. The model was validated using results derived from a design of experiments. Values of both, the electroosmotic drag coefficient and the methanol concentration within the cathode, were extracted from the model and compared to structural properties and operating conditions. The influence of temperature, membrane thickness, molarity and anode flow rate on methanol crossover was studied in detail. It was shown that Faraday efficiency can be improved at high cell current densities, thick membranes and near ambient temperatures. Methanol concentration and anode flowrate should be kept low to decrease crossover of methanol across the membrane.

References

[1] Frost & Sullivan, World Micro Fuel Cell Markets for Consumer Portable Devices, Market Engineering Research, Frost & Sullivan 2400 Geng Road, Suite 201 Palo Alto, CA 94303-3331, USA (05.10.2006 2006).
[2] www.HFPeurope.org, European Hydrogen & Fuel Cell Technology Platform: Strategic Research Agenda, Tech. rep. (2005).
[3] T.F. Fuller, J. Newman, J. Electrochem. Soc. 139 (5) (1992) 1332–1337.
[4] J.T.A. Zawodzinski, C. Derouin, S. Radzinski, R.J. Sherman, V.T. Smith, T.E. Springer, S. Gottesfeld, J. Electrochem. Soc. 140 (4) (1993) 1041–1047.
[5] J. Cruickshank, K. Scott, J. Power Sources 70 (1) (1998) 40–47.
[6] V. Gogel, T. Frey, Z. Yongsheng, K. Friedrich, L. Joerissen, J. Garche, J. Power Sources 127 (2004) 172–180.
[7] A. Heinzel, V. Barragan, J. Power Sources 84 (1) (1999) 70–74.
[8] S. Song, W. Zhou, W. Li, G. Sun, Q. Xin, S. Kontou, P. Tsiakaras, Ionics 10 (5-6) (2004) 458–462.
[9] A. Oedegaard, J. Power Sources 157 (1) (2006) 244–252.
[10] J.P. Meyers, J. Newman, J. Electrochem. Soc. 149 (6) (2002) A729–A735.
[11] H. Dohle, K. Wippermann, J. of Power Sources 135 (1–2) (2004) 152–164.
[12] B.L. Garcia, V.A. Sethuraman, J.W. Weidner, R.E. White, R. Dougal, J. Fuel Cell Sci. Technol. 1 (1) (2004) 43–48.
[13] K.T. Jeng, C.W. Chen, J. Power Sources 112 (2) (2002) 367–375.
[14] G. Murgia, L. Pisani, A.K. Shukla, K. Scott, J. Electrochem. Soc. 150 (9) (2003) A1231–A1245.
[15] Z. Wang, C. Wang, J. Electrochem. Soc. 150 (4) (2003) A508–A519.
[16] K. Wippermann, B. Richter, K. Klafki, J. Mergel, G. Zehl, I. Dorbandt, P. Bogdanoff, S. Fiechter, S. Kaytakoglu, J. Appl. Electrochem. 37 (12) (2007) 1399–1411.

[17] R.R. Barton, Graphical Methods for the Design of Experiments, Springer, 1999.
[18] B.L. Garcia, Kinetics and Mass Transfer in a Direct Methanol Fuel Cell, Dissertation, University of South Carolina, 2007.
[19] J.P. Meyers, J. Newman, J. Electrochem. Soc. 149 (6) (2002) A718–A728.
[20] S. Ma, M. Odgaard, E. Skou, Solid State Ionics 176 (39–40) (2005) 2923–2927.
[21] H. Dohle, J. Divisek, J. Mergel, H. Oetjen, C. Zingler, D. Stolten, J. Power Sources 105 (2) (2002) 274–282.
[22] A. Siebke, Modellierung und numerische simulation der direktmethanol-brennstoffzelle, Dissertation, Univ. Stuttgart, 2003.
[23] A. Kulikovsky, Electrochem. Commun. 4 (12) (2002) 939–946.
[24] G. Rosenthal, Modellierung einer direkt-methanol-brennstoffzelle mit hilfe eigens bestimmter parameter, Dissertation: Fortschritt-berichte vdi, reihe 3: Verfahrenstechnik * band 791, TU Clausthal, Clausthal-Zellerfeld, 2003.
[25] T. Schultz, K. Sundmacher, J. Membr. Sci. 276 (1–2) (2006) 272–285.
[26] K. Scott, W. Taama, J. Cruickshank, J. Power Sources 65 (1–2) (1997) 159–171.
[27] M. Ise, K.D. Kreuer, J. Maier, Solid State Ionics 125 (1–4) (1999) 213–223.
[28] J. Divisek, J. Fuhrmann, K. Gartner, R. Jung, J. Electrochem. Soc. 150 (6) (2003) 811–825.
[29] S. Ge, B. Yi, P. Ming, J. Electrochem. Soc. 153 (8) (2006) A1443–A1450.
[30] S. Hikita, K. Yamane, Y. Nakajima, JSAE Rev. 23 (1) (2002) 133–135.
[31] D. Hongli, R.T. Wilkie, J. Electrochem. Soc. 153 (3) (2006) A521–A526.